Check for updates

View Article Online
View Journal

Biomaterials Science

Accepted Manuscript

This article can be cited before page numbers have been issued, to do this please use: T. Nakajima, K. Sasaki, A. Yamamori, K. Sakurai, K. Miyata, T. Watanabe and Y. T. Matsunaga, *Biomater. Sci.*, 2020, DOI: 10.1039/D0BM00763C.

This is an Accepted Manuscript, which has been through the Royal Society of Chemistry peer review process and has been accepted for publication.

Accepted Manuscripts are published online shortly after acceptance, before technical editing, formatting and proof reading. Using this free service, authors can make their results available to the community, in citable form, before we publish the edited article. We will replace this Accepted Manuscript with the edited and formatted Advance Article as soon as it is available.

You can find more information about Accepted Manuscripts in the Information for Authors.

Please note that technical editing may introduce minor changes to the text and/or graphics, which may alter content. The journal's standard Terms & Conditions and the Ethical guidelines still apply. In no event shall the Royal Society of Chemistry be held responsible for any errors or omissions in this Accepted Manuscript or any consequences arising from the use of any information it contains.

ROYAL SOCIETY OF CHEMISTRY

rsc.li/biomaterials-science

View Article Online
DOI: 10.1039/D0BM00763C

A simple three-dimensional gut model constructed in a restricted ductal microspace induces intestinal epithelial cell integrity and facilitates absorption assays

Tadaaki Nakajima[a], Katsunori Sasaki[b], Akihiro Yamamori[b], Kengo Sakurai[b], Kaori Miyata[b], Tomoyuki Watanabe[b, †], Yukiko T. Matsunaga[a,*].

[a] Institute of Industrial Science, The University of Tokyo, 4-6-1 Komaba, Meguro-ku, Tokyo 153-8505, Japan

[b] Sumitomo Chemical, Co., Ltd., 27-1, Shinkawa 2-chome, Chuo-ku, Tokyo 104-8260, Japan

[†]Current address: Matsuura Yakugyo Co., Ltd., 24-21, Enjo-cho, Showa-ku, Nagoya 466-0054, Japan

* Correspondence to:
Yukiko T. Matsunaga, Ph.D.
Institute of Industrial Science, The University of Tokyo 4-6-1 Komaba, Meguro-ku, Tokyo 153-8505, Japan
Tel.: +81-3-5452–6470; Fax: +81-3-5452-6471
E-mail: mat@iis.u-tokyo.ac.jp

Published on 31 August 2020. Downloaded by The University of Tokyo on 9/16/2020 10:48:37 AM.

Biomaterials Science Accepted Manuscript

View Article Online
DOI: 10.1039/D0BM00763C

Published on 31 August 2020. Downloaded by The University of Tokyo on 9/16/2020 10:48:37 AM.

Abstract

The intestine acts as a center for nutrient and water absorption at the epithelium and plays an important role in immunity. Considering the complexity of its function and roles in living systems, a physiologically relevant gut *in vitro* model is desirable in both basic biology and the analysis of effects of some substances on functions of the gut; these analyses include the screening of drug and food candidates with regard to intestinal disorder at an early stage of medical development. In the present study, we constructed a three-dimensional (3D) gut model using human absorptive enterocytes (CACO-2 cells) by reconstitution of the gut epithelial sheet restricted on a high-reproducible ductal scaffold of collagen gel. Moreover, using the 3D gut model, we evaluated the morphology at cellular and tissue levels and conducted a phenotypic analysis of the intestinal physiological functions, which involved a permeability assay mimicking barrier disruption inducing inflammation and an absorption assay reflecting ingestive effects. The ductal structure, *in vivo*-like 3D epithelial structures, epithelial barrier, and effective absorptive function characterized the 3D gut model. The epithelial cells formed a villus-like buckling epithelium, vertical microvilli of increased density on the cell surface, and a crypt-like localized cell proliferating region. The mature shape of the epithelium may contribute to mimicking barrier function and effective absorption compared with that in the 2D gut model. Furthermore, we successfully mimicked the dextran sodium sulfate-induced epithelial barrier dysfunction as a trigger phenomenon of gut inflammation in the 3D gut model. The integrity of the epithelium and phenotypic analysis of the intestinal physiological functions in the simple and reproducible 3D gut model will allow for a drug screening system for assessing the effects on the functions of the gut epithelium from the lumen side.

Keywords

Gut; 3D model; microvilli; villus; crypt; absorption

Biomaterials Science Accepted Manuscript

View Article Online
DOI: 10.1039/D0BM00763C

Published on 31 August 2020. Downloaded by The University of Tokyo on 9/16/2020 10:48:37 AM.

1. Introduction

The intestine acts as a center for nutrient and water absorption at the epithelium and plays an important role in immunity via coordinating interaction among the epithelial barrier, immune cells, and microbiome.[1] Disturbances in the mechanisms of the barrier functions and altered gut microbiome are involved in inflammation, obesity, and metabolic disease in the gastrointestinal tract.[2,3] Furthermore, quantification of absorption and intestinal metabolism is critical for an accurate projection of human pharmacokinetics following ingestion.[4] Therefore, the development of an *in vitro* quantification system is necessary for analyzing the effects and toxicity of some substances on the gut functions (such as screening the drug and food candidates for diseases of the gut). A simple two-dimensional (2D) *in vitro* gut model has been developed for analyzing the effects and toxicity of drugs or foods in the absorption and barrier functions of the gut epithelium. Around the 1990s, the development of the 2D gut model had commenced using a culture system of gut epithelial cell line on the filter to divide the apical region (lumen side) and basal region (parenchymal side) of the cells.[5] The traditional 2D gut model is still being used in recent studies for analyzing the effects of food[6] and bacteria[7], and the toxicity of substrate to the gut epithelial cells.[8] The simple 2D models have been modified for shortened culture time[9], paracellular absorption[10] and co-culture with other types of cells (e.g. immune cells[11] and fibroblasts[12]). However, the 2D gut models have limited appendix for structure; therefore, it cannot induce 3D complex gut epithelial structures.

For the development of a gut microphysiological system (MPS) to analyze the functions of the gut epithelium, mimicking the gut epithelial 3D structure *in vitro* using a simple and reproducible method is one of the most important factors. The structure of the gut epithelium is composed of large numbers of self-renewing crypt-villus units. A villus is a structure of protrusion to the lumen side and mainly responsible for absorption by enterocytes for which microvilli are lined on the cell surface, and for the

Biomaterials Science Accepted Manuscript

View Article Online
DOI: 10.1039/D0BM00763C

Published on 31 August 2020. Downloaded by The University of Tokyo on 9/16/2020 10:48:37 AM.

secretion of mucus from the goblet cells.[13] The villus is covered by a single layer composing postmitotic differentiated columnar epithelial cells. Several experiments of cell lineage-tracing and organoid formation from a single stem cell have demonstrated that these differentiated cells in villus are derived from stem cells at an epithelial invagination surrounded by villus (termed as crypt) that occurs in self-renewal of adult mouse and human cells and during regeneration.[13,14] This brush border formed by the crypt-villus domains and microvilli on the cell surface contributes to the absorptive function via the amplification of the surface area.[15] The epithelial cells are polarized both in the villus and crypt, and the apical surface of enterocytes forms microvilli and a brush border to the lumen side, wherein various proteins necessary for nutrient absorption and digestion are accumulated.[16]

To mimic the structure and function of a more natural gut organ, some types of gut-on-a-chip have been established using bioengineering techniques such as bio-microelectromechanical systems (BioMEMS), microfluidics, and tissue engineering. In one of the most effective experiments of gut-on-a-chip, the application of peristalsis-like movements and flow induces villus-like buckling epithelial sheet, crypt-like localized cell proliferating region, high epithelial thickness, and expression of some proteins in the differentiated cells.[17–20] The chip facilitates the evaluation of the effects of co-cultured bacteria on the barrier function, gene expression, and structure of the gut epithelial sheet using a single strain[17,19] or microbiome.[20] Furthermore, using dextran sodium sulfate (DSS) that induces ulcerative colitis in mouse model[21], the epithelial barrier function was controlled as an inflammatory milieu in the gut-on-a-chip.[22] The porous hollow fibers of polyethersulfone allow the ductal shape culture of gut epithelial cells and accelerate the expression of intestine functions.[23] Combination of tubular shape on the stroma equivalent composing gelatin and myofibroblasts, peristaltic-like motion and air-liquid interface induces villus-like buckling and region-specific differentiation of the gut epithelial cells.[24] The ductal scaffold composed of silk protein sponge matrices enables the crosstalk of co-cultured immune

Biomaterials Science Accepted Manuscript

View Article Online
DOI: 10.1039/D0BM00763C

Published on 31 August 2020. Downloaded by The University of Tokyo on 9/16/2020 10:48:37 AM.

cells with the gut epithelial cells, resulting in the establishment of an inflammatory response that can be visualized in the 3D gut model.[25] However, special substrates or power supplies are required for those 3D gut models, and no system allowed both the induction of 3D epithelial structure and co-culture with immune cells. Additionally, no system has evaluated the absorption values of foods and drugs via the gut epithelial sheet from the apical lumen side similar to the 2D gut model.

We attempted to mimic the developmental process in gut-on-a-chip for constructing a 3D gut structure *in vitro*. In the developmental stage, an expansion of the epithelial sheet at the restricted ductal region using a smooth muscle layer generates compressive stress to itself, and the stress is necessary and sufficient for the induction of a epithelial buckling and folding structure of villus.[26] The report suggests that the design of microspace is important for the formation of 3D epithelial structure in the gut-on-a-chip by the aspect of development. In this study, we considered the reconstitution of gut epithelial sheet that is restricted on the ductal scaffold of collagen gel designed using polydimethylsiloxane (PDMS) chip and needle. The 3D gut model was characterized by the ductal structure, *in vivo*-like 3D epithelial structures, epithelial barrier, and effective absorptive function. The epithelial cells formed a villus-like buckling epithelium, vertical microvilli of an increased density on the cell surface, and a crypt-like localized cell proliferating region. The mature shape of the epithelium may contribute to mimicking the barrier function and effective absorption compared with that in the 2D gut model.

2. Materials and methods

2-1. Cell culture

A human colon adenocarcinoma cell line—CACO-2 cells—was obtained from RIKEN BRC (Tsukuba, Japan; NO. RCB0988) and cultured in Eagle's minimum essential medium (FUJIFILM Wako, Osaka, Japan) containing 20% fetal bovine serum (Biosera, Nuaille, France), 1% MEM non-essential

Biomaterials Science Accepted Manuscript

View Article Online
DOI: 10.1039/D0BM00763C

Published on 31 August 2020. Downloaded by The University of Tokyo on 9/16/2020 10:48:37 AM.

amino acid solution (FUJIFILM Wako) and 1% penicillin—streptomycin solution (FUJIFILM Wako) in a humidified atmosphere of 5% CO_2 at 37°C. The cells were passaged using 0.25% (w/w) trypsin—5.3 mM EDTA solution (FUJIFILM Wako). The cells were filtered through a 35 μm cell strainer (Corning, Corning, NY, USA) to dissociate cell aggregates and then counted via trypan blue staining using a hemocytometer before using 2D and 3D gut models.

2-2. Preparation of the 2D gut model

We slightly modified the traditional method of the 2D gut model.[5] Fibronectin solution (10 μg/mL; FUJIFILM Wako) was poured into the inner Falcon cell culture inserts (PET membrane; pore sizes, 0.4 μm diameter; Corning) placed into a 12-well plate and incubated at 37°C for 10 min. To initiate the culture at confluent state, 1×10^5 CACO-2 cells were seeded on the membrane and cultured in 1 mL medium of each well and insert in a humidified atmosphere of 5% CO_2 at 37°C for 16 days with the medium being changed every other day.

2-3. Preparation of the 3D gut model

The polydimethylsiloxane (PDMS)-based chips (25×25×5.0 mm: width×length×height) which included needle-inserting channels (250 μm square) on both sides were used. The construction method for the 3D microvessel model has previously been described[27–29], and we modified the method to construct the 3D gut model. The PDMS chip was treated with O_2 plasma. An acupuncture needle (300 μm diameter; Seirin, Shizuoka, Japan) was coated with phosphate-buffered saline (PBS) containing 1% (w/w) bovine serum albumin (BSA; Sigma-Aldrich, St Louis, MO, USA). Eight volumes of Cellmatrix type I-A (Nitta Gelatin, Osaka, Japan) were mixed with 1 volume of 10×Hanks' buffer (Sigma-Aldrich), following which 1 volume of 200 mM HEPES buffer (containing 262 mM $NaHCO_3$ and 0.05 N NaOH) was added to the

Biomaterials Science Accepted Manuscript

View Article Online
DOI: 10.1039/D0BM00763C

Published on 31 August 2020. Downloaded by The University of Tokyo on 9/16/2020 10:48:37 AM.

mixture. This cold mixture was poured into the circular wells of both sides and the center chamber (square well, 6.0×2.5×2.0 mm: width×length×height). The BSA-coated needle was inserted via the PDMS channel. The mixture was allowed to gel at 37°C for 90 min, resulting in the formation of a hollow channel upon withdrawal of the needle. The channel was coated with 10 μg/mL fibronectin solution at 37°C for 10 min. CACO-2 cells were harvested and resuspended in medium containing 3% dextran (from *Leuconostoc* spp. M_r 450,000-650,000; Sigma) at a density of 4×10^6 cells/mL. The suspension was loaded from side wells to the hollow channel and the cells were incubated in a humidified atmosphere of 5% CO_2 at 37°C for 20-30 min. This step was then repeated. After confirmation of cell adhesion at the confluent state, the remaining suspended cells were flushed by loading the medium. The 3D gut model was cultured in 1 mL medium in a humidified atmosphere of 5% CO_2 at 37°C for 16 days with flushing to remove the remaining dead cells and medium change every other day. The bright-field images were captured by a fluorescent microscope (Axio observer Z1, Carl Zeiss, Oberkochen, Germany) equipped with a 20× observation lens (LD Plan-Neofluar 20×/0.4 Korr Ph 2 M27).

2-4. Optical coherence tomography (OCT) imaging

Label-free 3D imaging of the gut model (n=3-5 in 2D, n=9-12 in 3D, biologically independent) was performed with OCT using a Cell3 iMager Estier (SCREEN, Kyoto, Japan) as described previously.[30] The images were processed with ImageJ (National Institutes of Health, Bethesda, MD, USA).

ImageJ was used to analyze the ductal diameter and epithelial thickness. By randomly selecting 3 pictures per sample, the diameter of the major and minor axes and epithelial thickness at 4 regions (top, bottom, and both lateral sides) were measured. All the values were averaged for one sample data.

2-5. Transmission electron microscopy (TEM)

Biomaterials Science Accepted Manuscript

View Article Online
DOI: 10.1039/D0BM00763C

Published on 31 August 2020. Downloaded by The University of Tokyo on 9/16/2020 10:48:37 AM.

The 2D and 3D gut samples (n=3, biologically independent) were fixed with 2.5% glutaraldehyde in PBS and post-fixed with 2% osmium tetroxide in PBS at 4°C for 2 h. The samples were dehydrated with an ascending series of ethanol and acetone, following which they were embedded with epoxy resin. Cross-sections with 1 μm thickness were prepared and stained with hematoxylin and eosin or toluidine blue to confirm the whole image and decide the area for TEM under the light microscope. The ultra-thin sections were prepared and stained with 2% hafnium and 0.15% lead citrate for TEM. Six images were randomly captured in each sample. The cellular height and aspect ratio (height/width) of CACO-2 cells were measured in the TEM images using ImageJ. For analyzing of cellular height, 3 cells were randomly selected in an image, and the mean of the 18 cells was used as data for a sample. For analyzing aspect ratio, 10 cells were randomly selected. To analyze the area of microvilli, the TEM images were binarized, an area of 1 μm height from the top of the cell surface was selected, and the %area of microvilli was measured. To detect the vertical level of microvilli, 10 microvilli were randomly selected in an image, and the absolute angles from the surface of the cells (0°-90°) were measured.

2-6. EdU cell proliferation assay

The 2D and 3D gut model samples cultured for 16 days (n=3, biologically independent) were treated with 20 μM EdU-containing medium for 24 h and then fixed by 4% (w/w) paraformaldehyde (PFA; FUJIFILM Wako) in PBS for 30 min. The samples were washed with PBS and 3% (w/w) BSA/PBS and then permeabilized in 0.5% (v/v) Triton X-100 (Sigma-Aldrich)/PBS at room temperature (R.T.) for 15 min. After washing with 3% BSA/PBS, the samples were incubated in reaction cocktail of Click-iT EdU Cell Proliferation Kit for Imaging, Alexa Fluo 594 dye (Thermo Fisher Scientific, Waltham, MA, USA) as per manufacturer's instructions at R.T. for 60 min. After washing with 3% BSA/PBS, the nuclei were stained using Hoechst 33342 at R.T. for 15 min. The samples were washed with PBS

Biomaterials Science Accepted Manuscript

View Article Online
DOI: 10.1039/D0BM00763C

Published on 31 August 2020. Downloaded by The University of Tokyo on 9/16/2020 10:48:37 AM.

containing 0.1% (v/v) Tween 20 (PBST) 8 times and incubated in PBST at 4°C overnight. After washing with PBS, the EdU-positive cells were observed using a confocal microscope (LSM 700, Carl Zeiss) equipped with a 40× water-immersion detection objective lens (LD C-Apochromat 40×/1.1W Korr M27). The images were binarized by Imaris software (Bitplane, Zurich, Switzerland).

The number of EdU-positive and Hoechst-positive cells was counted, and the distribution of the EdU-positive cells in the maximum intensity projection images was calculated using ImageJ. To calculate the distribution, the images were divided into 9 sub-areas, the EdU-positive cells were counted in the sub-areas, and the values of χ^2 were calculated using the equation provided ahead. The p values were directly calculated using the values of χ^2 with χ^2 test:

$$\chi^2 = \frac{\sum_{i=1}^{9}(x_i - \bar{x})^2}{\bar{x}}$$

2-7. Immunofluorescence

The 2D and 3D gut model samples cultured for 16 days (n=3, biologically independent) were fixed by 4% PFA/PBS for 30 min and permeabilized with 0.5% Triton X-100/PBS at R.T. for 10 min. After washing with PBS, blocking was performed with 1% BSA/PBS at 4°C overnight. The samples were then incubated with primary antibodies in 1% BSA/PBS at 4 °C overnight. The used primary antibodies were rabbit monoclonal anti-human villin antibody [SP145] (Abcam, Cambridge, UK; 1:100) and mouse monoclonal anti-human lysozyme antibody [BGN/06/961] (Abcam; 1:100) or rabbit polyclonal anti-ZO1 antibody [40-2200] (Thermo Fisher Scientific; 1:200). After incubation with a secondary antibody or Alexa Fluor 488 phalloidin (Thermo Fisher Scientific) at 4°C overnight, the nuclei were stained with Hoechst 33342. The images were obtained using an LSM 700 equipped with a 40× water-immersion detection objective lens and 3D-binarized using Imaris software. The F-actin area in the maximum

Biomaterials Science Accepted Manuscript

View Article Online
DOI: 10.1039/D0BM00763C

intensity projection images was measured by binarization using ImageJ.

2-8. RNA isolation and quantitative reverse transcript (qRT)-PCR

Total RNAs of the 2D and 3D gut model samples were extracted by ISOGEN (Nippon Gene, Tokyo, Japan) (n=4, biologically independent). cDNA was synthesized from 1 μg/10 μL RNA using ReverTra Ace qPCR RT Master Mix (TOYOBO, Osaka, Japan). Real-time PCR was performed using the StepOnePlus real-time PCR system (Applied Biosystems; Thermo Fisher Scientific) with THUNDERBIRD SYBR qPCR Mix (TOYOBO) according to the manufacture's protocol. The primer sets for actin beta (*ACTB*), leucine rich repeat containing G protein-coupled receptor 5 (*LGR5*), lysozyme (*LYZ*), mucin 2 (*MUC2*) and villin 1 (*VIL1*) were derived from the GenBank sequences (Table S1). For quantification, the target genes were normalized to the internal standard gene, ACTB, and the level of mRNA of each gene in the 2D gut model were applied for the standard (relative expression=1).

2-9. Permeability assay

For permeability assay, the 3D gut model was treated with 2% (w/w) dextran sodium sulfate (DSS) MW36,000-50,000 (FUJIFILM Wako) in medium from 12 to 16 days of culture (n=3, biologically independent). The samples were set up on fluorescent microscope (Axio observer Z1) in an incubation chamber that maintained a humidified atmosphere of 5% CO_2 at 37°C (INU Incubation System for Microscopes–model WSKM, Tokai Hit, Fujinomiya, Japan). The 2D or 3D samples were applied with 200 or 7 μL of 200 μg/mL FITC-dextran (4 kDa; Sigma-Aldrich) in the medium on the insert or from the lumen side, respectively. The images were obtained using the Axio observer Z1 having a 20× observation lens every 10 min with a FITC-dextran-added medium change every 20 min. After observation, the samples were fixed for immunofluorescence for ZO1. The fluorescent intensity was analyzed in the

Published on 31 August 2020. Downloaded by The University of Tokyo on 9/16/2020 10:48:37 AM.
Biomaterials Science Accepted Manuscript

View Article Online
DOI: 10.1039/D0BM00763C

Published on 31 August 2020. Downloaded by The University of Tokyo on 9/16/2020 10:48:37 AM.

200×1000 μm squares at a distance of 50 μm from the edge of the gut using ImageJ.

2-10. Absorption assay

The 2D and 3D gut model samples cultured for 16 days (n=4, biologically independent) were washed twice with Hanks' buffer (pH 6.0; FUJIFILM Wako) and incubated at 37°C for 30 min. After washing with Hanks' buffer, 500 or 10 μL 0.5 mM α-lipoic acid (αLA; Sigma) in pH 6.0 Hanks' buffer with or without 10 mM NaN_3 was applied on the insert or from the lumen side in the 2D or 3D samples, respectively. In the 2D samples, 1 mL of pH 6.0 Hanks' buffer was poured into the well. After incubation at 37°C for 30 min, the buffer in the wells of 2D samples was collected for mass spectrometry (MS), and leakage via simple diffusion was then checked in the 2D and 3D samples as described ahead. In the 3D samples, the lumen was washed with pH 6.0 Hanks' buffer 3 times, and the collagen gel was collected for MS.

The αLA level in Hanks' buffer of the 2D samples and in collagen gel of the 3D samples were measured using the Prominence UFLC system (Shimadzu Co., Kyoto, Japan) coupled to a Thermo TSQ Vantage triple quadrupole mass spectrometer (Thermo Fisher Scientific, Bedford, MA, USA) with a heat electrospray ionization (H-ESI) source. The UFLC conditions were as follows: ultraviolet absorption detection wavelength, 254 nm; analytical column, COSMOSIL 3C18-EB Packed Column (Nacalai Tesque, Inc., Kyoto, Japan); and mobile phase, gradient elution with 0.1% formic acid in acetonitrile. The operating conditions of H-ESI positive MS were as follows: spray voltage, 3000 V; vaporizer temperature, 400°C; sheath gas flow rate, 50 arb; aux gas flow rate, 15arb; and capillary temperature, 250°C. The detected analyte ions include precursor ion (*m/z*: 205), which was converted to product ion (*m/z*: 171). Before analysis, the buffer solution of the 2D samples was diluted 20 times with acetonitrile, and the collagen gel of the 3D samples was extracted with 100 μL of acetonitrile, well stirred with a vortex mixer,

Biomaterials Science Accepted Manuscript

View Article Online
DOI: 10.1039/D0BM00763C

Published on 31 August 2020. Downloaded by The University of Tokyo on 9/16/2020 10:48:37 AM.

and centrifuged. The diluted solution and supernatants were subjected to the analysis.

To examine leakage, the samples were set up on the Axio observer Z1 in an incubation chamber that maintained a humidified atmosphere of 5% CO_2 at 37°C. The 2D or 3D samples were applied with 200 or 7 μL of 200 μg/mL FITC-dextran (4 kDa) in the medium on the insert or from the lumen side, respectively. In the 2D samples, a new 1 mL of pH 6.0 Hanks' buffer was poured in the well. The images were obtained using the Axio observer Z1 with a 20× observation lens at 20 min after the application.

2-11. Statistics

Data were expressed as mean ±standard deviation (S.D.). For single comparison, two-tailed Student's *t*-test or Welch's *t*-test was used. For multiple comparisons, differences were estimated using a one-way Peritz or Games—Howell test. A statistically significant difference was defined as $p \leq 0.05$.

3. Results

3-1. Construction of 3D gut model using simple PDMS chip

We developed the methods of the 3D gut model using a simple PDMS chip (Fig. 1A). The collagen solution was poured into the PDMS chip and the needle was inserted. Following gelation, the needle was withdrawn to form a hollow channel as a ductal collagen gel scaffold (φ = 300 μm). CACO-2 cell suspension was loaded to the hollow channel, and the cells were incubated to induce cell adhesion. A three-step experimental scheme was designed in this study: (i) construction of a 3D gut model on the restricted ductal scaffold of collagen gel using a simple PDMS chip, (ii) evaluation of the morphology at the cellular and tissue levels, and (iii) establishment of phenotypic analysis systems for assessing barrier and absorptive functions (Fig. 1B). Because the side wells were connected to the lumen and separated from the center chamber, we could apply some factors (e.g. fluorescent substance and αLA) only to the

Biomaterials Science Accepted Manuscript

View Article Online
DOI: 10.1039/D0BM00763C

lumen and then analyze barrier and absorptive functions solely from the lumen side.

(Insert Fig. 1 here)

Published on 31 August 2020. Downloaded by The University of Tokyo on 9/16/2020 10:48:37 AM.

In the 3D gut model thus prepared, the ductal diameter and epithelial layer thickness increased with increase in culture time (Fig. 2A). The thickened epithelium appeared to form a buckling structure at 16 days of the culture period (Fig. 2A and B, arrows). To confirm the detailed epithelial structure, the 3D observation was performed using the OCT imaging system[30] that allows 3D time-lapse imaging without fluorescent cell labeling (Fig. 2C). The epithelium formed a buckling structure at 16 days in the 3D image (arrows), and clear buckling was often detected in the vertical plane (i.e. along the ductal axis). On the other hand, the epithelium was smooth in the 3D model from 4 to 12 days and the 2D model. After culture, the ductal diameter decreased from the original lumen diameter by 300 μm and significantly increased with the culture and return to the original size at 16 days (Fig. 2D). The mean value and S.D. of the epithelial thickness increased with the culture, indicating the ruggedness of the epithelium (Fig. 2E). Furthermore, the epithelium in the 3D model was significantly thicker than that in the simple 2D model in which the cells were cultured on the filter membrane using a conventional method (Fig. 2C and E). These results suggest that the epithelial cells differentiated from squamous cells into columnar cells and that the epithelial layer did not form a single and flat plane in the 3D gut model.

(Insert Fig. 2 here)

3-2. Formation of villus- and crypt-like domains in the 3D gut model

Induction of positional differentiation of CACO-2 cells was analyzed in the buckling epithelium of

Biomaterials Science Accepted Manuscript

View Article Online
DOI: 10.1039/D0BM00763C

Published on 31 August 2020. Downloaded by The University of Tokyo on 9/16/2020 10:48:37 AM.

the 3D gut model because the cells mainly differentiated into 2 types—invaginating crypt- and protrusive villus-consisting cells—in the gut epithelium *in vivo*. After culture for 16 days, several EdU-positive proliferating cells were detected in the 3D model; however, there were few in the 2D model (Fig. 3A and B; Fig. S1A). To evaluate the localization of proliferating cells in the epithelial tissue, maximum intensity projection images were divided into 9 sub-images, and the values of χ^2 were calculated. The high or low values of χ^2 indicated localized or uniform distribution of the proliferating cells, respectively. High values of χ^2 in the 3D model indicated that the proliferating cells were significantly localized (the *p* values were directly calculated from the values of χ^2) (Fig. 3C). In the 2D gut model, stress actin fibers were detected only in the region between the cells. On the other hand, the expression of stress actin fibers was significantly higher in the 3D gut model, and those were mainly detected entirely at the basal side in the epithelial cells after culture for 16 days (Fig. 3D and E). The localization of protein expression of villin was confirmed at the cell surface of the entire epithelium, and the *VIL1* mRNA expression was not different between the 2D and 3D gut model (Fig. S1B; Fig. 1F) Lysozyme was mainly expressed at the bottom zone in the 2D and 3D models, and the *LYZ* mRNA expression in the 3D gut model was higher than that in the 2D gut model. MUC2 protein was not detected in the 2D and 3D gut models, and the mRNA expression was not different between the 2D and 3D gut model. The expression of the stem cell marker gene in the crypt—LGR5—was high in the 3D gut model. These results of marker protein and gene expression suggested that the CACO-2 cells in the 3D gut model may be differentiated to Paneth cells and converted to stem cells in the crypt-like structure models. Taken together, the 3D gut model tends to induce separated crypt- and villus-like epithelial domains within the buckling epithelial tissue (Fig. 3G).

(Insert Fig. 3 here)

Biomaterials Science Accepted Manuscript

View Article Online
DOI: 10.1039/D0BM00763C

Published on 31 August 2020. Downloaded by The University of Tokyo on 9/16/2020 10:48:37 AM.

3-3. Epithelial differentiation at the cellular level in the 3D gut model

We evaluated details of epithelial cell differentiation in the 3D gut model using TEM. In all the samples of the 2D and 3D models cultured for 4 or 16 days, CACO-2 cells were completely attached to the filter or collagen gel and made an epithelial sheet with a cellular junction and microvilli were present at the cell surface of the lumen side (Fig. 4A and B). Several microvilli were detected lined on the cell surface in the lumen side at 16 days of culture only in the 3D model (Fig. 4A). A clear tight junction was detected in the 3D model cultured for 4 days but not in the 2D model (Fig. 4B, yellow boxes). The tight junction was formed both in 2D and 3D models cultured for 16 days (Fig. 4B, yellow boxes). The height of epithelial cells in the 3D model was significantly higher than that in the 2D model cultured both for 4 and 16 days (Fig. 4C). Furthermore, the cell aspect ratio (height/width) was 0.29 ± 0.04 in the 2D model and 0.91± 0.25 in the 3D model (Fig. 4D), indicating that the shape of the cells was similar to squamous and cuboidal epithelial cells in the 2D and 3D models, respectively. A significant increase in the density of microvilli on the cell surface was observed only in the 3D model cultured for 16 days (Fig. 4E). The angles of microvilli were widely distributed in the 2D model, indicating that the microvilli were misaligned (Fig. 4F). Conversely, in the 3D model, the distribution of angles was drastically shifted into a 90°, indicating that the microvilli were vertically aligned after culture for 16 days (Fig. 4F). The mean values of the angles indicated that the microvilli in the 3D model were vertical type compared with that in the 2D model both at 4 and 16 days (Fig. 4G). Overall, CACO-2 cells in the 3D gut model morphologically differentiated into *in vivo*-like gut epithelial cells that expressed early tight junction formation, high cellular height, high aspect ratio (height/width), and vertical microvilli lining on the surface (Fig. 4H).

Biomaterials Science Accepted Manuscript

View Article Online
DOI: 10.1039/D0BM00763C

(Insert Fig. 4 here)

Published on 31 August 2020. Downloaded by The University of Tokyo on 9/16/2020 10:48:37 AM.

3-4. Establishment of permeability and absorption assay system using the 3D gut model

To explore the potential applications of the 3D gut model in the use of intestinal physiological function assay, we performed a phenotypic analysis of barrier and absorptive functions. DSS treatment induces ulcerative colitis in mouse inflammation model[21], and this treatment is used to induce the epithelial barrier dysfunctions as a trigger phenomenon of gut inflammation in the gut-on-a-chip.[22] Therefore, we attempted to mimic epithelial barrier dysfunctions by DSS treatment in the 3D gut model. The treatment of 2% DSS from 12 to 16 days of culture reduced the height and disrupted the buckling structure of the epithelium in the 3D model (Fig. 5A). Any leakage of the FITC-4 kDa dextran in the medium from the lumen to the collagen gel was not detected within 120 min in the 3D model, but DSS treatment significantly induced the increase of leakage in a time-dependent manner (Fig. 5A and B). In the 2D model, although the increase of leakage was immediately detected by DSS treatment, the fluorescent intensity was not increased with time course (Fig. 5B); therefore, the epithelial barrier dysfunctions were not observed in the 2D model following DSS treatment. The protein consisting of tight junction ZO1 was expressed at the cell border in the 2D and 3D models (Fig. 5C). The DSS treatment disrupted the expression pattern of this protein in the 3D model, and the effect was slight in the 2D model. Therefore, we successfully mimicked the DSS-induced epithelial barrier dysfunctions as a trigger phenomenon of gut inflammation in the 3D gut model.

Further, we developed an absorption assay system with MS. Any leakage of FITC-dextran in the buffer from the lumen to the collagen gel was not detected within 120 min in the 3D model, but weak leakage was detected under the filter membrane at this time in the 2D model (data not shown). At 4 days

Biomaterials Science Accepted Manuscript

View Article Online
DOI: 10.1039/D0BM00763C

Published on 31 August 2020. Downloaded by The University of Tokyo on 9/16/2020 10:48:37 AM.

in the 3D model, leakage from the lumen side was detected between the PDMS device and collagen gel (Fig. S2A, arrows); therefore, absorption of αLA for 30 min was detected in the gut models cultured for 16 days. After the absorption assay, no leakage via simple diffusion was confirmed following FITC-dextran treatment both in 2D and 3D models cultured for 16 days (Fig. S2A and B). The 3D model realized significantly higher absorption of αLA per unit area than that showed by the 2D model when the 2D and 3D models were hypothesized as a simple sheet and duct, respectively (Fig. 5D). The absorption was derived from active biological transport because NaN_3 co-treatment significantly decreased the αLA volume. Therefore, we newly established a more effective absorption analysis than the traditional ones, and one of the reasons for this increased efficacy was the increase of cell surface area by a high density of microvilli and buckling epithelium (Fig. 5E).

(Insert Fig. 5 here)

4. Discussion

We established a completely covered gut epithelial sheet on the 3D ductal scaffold of collagen gel using simple method without using special substrates or a power supply. The epithelial sheet had a villus-like buckling shape, vertical microvilli lining on the cell surface, complete barrier functions, and effective absorptive function. The 3D gut model would be useful for high-throughput drugs and food screening to analyze the effects on gut epithelial functions.

It is a biologically important finding that a 3D culture system on a ductal scaffold of collagen gel induced the formation of buckling structure of the gut epithelium at the tissue level and the differentiation of columnar epithelial cells and microvilli at a cellular level. The complex structure of epithelium is observed in the gut and in various types of ductal organs, and it is induced by numerous physical and

Biomaterials Science Accepted Manuscript

View Article Online
DOI: 10.1039/D0BM00763C

Published on 31 August 2020. Downloaded by The University of Tokyo on 9/16/2020 10:48:37 AM.

biological factors. In the gut, the restriction of the epithelial region by the formation of circular smooth muscle layer and peristalsis are the candidates of the physical factors for the induction of the epithelial structure at the tissue level. In the organ culture of gut tissue extracted from the smooth muscle layer, the epithelium develops as a simple smooth layer; however, only regional restriction using a scaffold of 300 μm diameter induces the epithelial buckling, indicating that regional restriction is sufficient for the induction of gut epithelial buckling.[26] The inhibition or activation of peristalsis does not affect the epithelial formation in this stage[26], indicating that the pressure of peristaltic contraction is not required for the initiation of the buckling structure in the development of the gut. In mathematical models, the epithelial cell proliferation in the restricted region by the ductal structure induces epithelial buckling and controls the shape (e.g. direction of buckling).[31] In the sphere scaffold of alginate gel, the forces acting within the epithelial monolayer were determined by measuring the elastic deformation, indicating that the compressive stress arising from epithelial cell proliferation is indeed sufficient to induce the buckling structure.[32] Furthermore, the apical stiffness of the epithelial sheet and external resistance control the size and number of the buckling structure.[33] These reports have hypothesized that the complexity of ductal epithelial structure is commonly derived from compress stress and from the difference in stiffness at the apical–basal axis of the cells caused via the restriction of the region. We simply demonstrated this theory using only the gut epithelial cell line and the ductal scaffolding of collagen gel. In the 3D gut model, stress fibers heterogeneously expressed at the basal side at the epithelial sheet (Fig. 3D and E), suggesting that compressive stress occurred in the epithelial duct. Analysis of the dynamics of the local pressure within the epithelial sheet would be interesting.

Heterogeneity of compressive stress induced by the buckling structure or ductal scaffold may involve in localized cell proliferating regions like a crypt. The structure of crypt is formed by apical contraction derived from stress fiber and myosin at the epithelial cells after birth.[34] Hippo/Yes-associated

Biomaterials Science Accepted Manuscript

View Article Online
DOI: 10.1039/D0BM00763C

Published on 31 August 2020. Downloaded by The University of Tokyo on 9/16/2020 10:48:37 AM.

protein (YAP) pathway activated RhoA is essential for cell proliferation and regeneration of crypt and buckling epithelial structures.[35–38] Furthermore, the YAP signaling pathway is important for crypt-villus-like asymmetric differentiation from single stem cells in the intestinal organoids.[39] The YAP signaling is reduced by a compositional change of actin fiber derived from compressive stress.[40] In the 2D dense epithelial sheet, the cells are cultured under the homogeneous compressive stress[40]. In the present study, few stress fibers were confirmed in the 2D gut model. These studies suggest that low cell proliferative ratio in the 2D gut model may be caused by the homogeneous compressive stress and low YAP signaling. Further, the YAP signaling is one of the candidates to control cell proliferation by the heterogeneity of compressive stress in the 3D gut model. Cell proliferating regions were localized and *LGR5* and *LYZ* expression was increased, suggesting that the 3D gut model may include the crypt-like phenotype. However, the expression of differentiation marker for enterocyte and goblet cell—VIL1 and MUC2—was not clearly different in the 2D and 3D gut models at this time; therefore, the cell differentiation for those at villus region rarely occurred. Peristalsis-like motion induces regional differentiation revealed as the expression of specific marker proteins.[18,24] Therefore, peristalsis might be important to induce further regional gut epithelial differentiation in this 3D gut model.

At a cellular level, the restricted cell region by ductal scaffolding of collagen gel induced the formation of apical polarity represented by vertical microvilli lining, columnar cell-like aspect ratio, and early tight junction formation. Apical contraction is one of the important factors for the induction of microvilli in the renal epithelial cell sheet.[41] Inhibition of the myosin contraction reduces the aspect ratio (height/width) of epithelial cells in the epididymal duct.[42] Therefore, apical contraction and compressive stress formed by the restricted region of the ductal scaffold are involved in both apical polarization and formation of columnar cell shape. However, the apical polarization is not induced in single intestinal epithelial cells cultured on collagen gel but is induced on Matrigel via the activation of RhoA signaling.[43]

Biomaterials Science Accepted Manuscript

View Article Online
DOI: 10.1039/D0BM00763C

Published on 31 August 2020. Downloaded by The University of Tokyo on 9/16/2020 10:48:37 AM.

The cellular height cultured on 2D hydrogel is 2-fold higher than that on the glass, and the 3D structure enhances this increase.[44] These reports suggest that soft scaffold or its composition is sufficient to induce apical polarization and columnar cell shape formation in gut epithelial cells and that compressive stress in the epithelial sheet enhances these events. Tight junction formation was earlier in the 3D gut culture on the ductal scaffold than in the 2D culture. The cell–cell junction may cause no leakage following long-term incubation in the buffer in the 3D gut model. Overall, simple 3D culture on a ductal scaffold of collagen gel induced epithelial sheet integrity including a mature structure at the tissue level, complete barrier function, and lined microvilli formation at the polarized apical surface. The integral gut epithelial structure increased the apical surface area per unit area by buckling and microvilli compared with that in flat plane, thereby increasing the absorption of αLA.

In previous studies, the 3D gut culture systems have been developed using some methods, but highly reproducible ductal lumen on the scaffold of the soft gel has not been applied to the methods. In a gut-on-a-chip using peristalsis-like motion, the compressive stress induces buckling epithelial structure and cell proliferating region localization.[17,18] However, in the development *in vivo*, the buckling epithelial structure is induced by the compressive stress derived from regional restriction rather than peristalsis.[26] In mouse gut development, circular contraction is weak at embryonic day 7 (E7) and rhythmically occurs from E10.[45] Longitudinal peristalsis is initiated from E13.5 independently of innervation, and rhythmic peristalsis is detected after birth.[46] The buckling structure is induced from E11.5 in mouse[26]; therefore, the late occurrence of the peristalsis may be one of the reasons for the requirement of the restricted region for buckling in development, and the peristalsis-induced compressive stress may enhance the elongation of the villus- and crypt-domains *in vivo*. Flow is another factor that enhances the elongation of the structure.[47] Therefore, we induced buckling structure in simple *in vitro* culture system in mimicking *in vivo* development.

Biomaterials Science Accepted Manuscript

View Article Online
DOI: 10.1039/D0BM00763C

Published on 31 August 2020. Downloaded by The University of Tokyo on 9/16/2020 10:48:37 AM.

The co-culture of gut epithelial cells with both bacteria and immune cells indicates the establishment of an evaluation system of an inflammatory response *in vitro* gut-on-a-chip. The co-culture system with bacteria has been developed in peristalsis-induced 3D gut epithelium cultured on membrane.[19,20] To co-culture with immune cells in the stromal region, the use of biomaterial scaffold is a simple solution. In fact, a co-culture system of gut epithelial cells has been developed with immune cells using the ductal scaffold composed of silk protein sponge matrices in the stromal region of scaffold.[25] The 3D duct model is not completely covered by the gut epithelial cells. Complete barrier function in the gut epithelial sheet is required for inflammatory analysis because the inflammatory inducers are treated from the lumen side in this analysis. Using the completely covered 3D gut model having no leakage from lumen to scaffold, we successfully mimicked the triggering phenomenon of inflammation—epithelial barrier dysfunction—via DSS treatment.

5. Conclusions

The newly developed 3D gut model has several significances in terms of epithelial functions and structures compared with the traditional 2D gut model. The epithelial sheet cultured on the new 3D gut model had integrity in epithelial shape, barrier, absorption, cell shape, and polarization using only regional restriction by the ductal scaffold of collagen gel. Unprecedentedly, we established an analysis system for assessing absorptive functions in the 3D gut model and the efficiency of absorption was higher than that in the 2D model. This simple 3D gut model has several applications in combination with other culture systems in the future. A combination of other physical treatment systems (e.g. peristalsis-like movement and flow) may have the potential to mimic a more natural *in vivo* villus-crypt-like structure. The 3D gut model facilitates co-culture with bacteria and immune cells because biomaterial soft gel as a scaffold can include other types of cells and the completely covered epithelial sheet can inhibit bacterial infiltration to

Biomaterials Science Accepted Manuscript

View Article Online
DOI: 10.1039/D0BM00763C

Published on 31 August 2020. Downloaded by The University of Tokyo on 9/16/2020 10:48:37 AM.

the parenchymal region. In the present study, CACO-2 cells, the gut epithelial cell line, was used for the 3D gut model. Intestinal stem cells maintained in the niche at crypt can be cultured to form self-organizing crypt-villus organoids.[48] From the human embryonic stem cells and the induced pluripotent stem cells, mature intestinal cells are induced as organoids and xenografts containing crypt-villus domains.[49,50] The structure of organoids can be controlled by the design of scaffold matrices.[51] However, because these organoids form the apical region and the lumen at inside of them, the treatment of some substrates from the lumen side is difficult. For application from the lumen side, the crypt-villus-like positional differentiation of the organoids can be re-organized on the 2D monolayers.[52] The organoids have been applied to the several platforms of organ-on-a-chip.[53,54] Recently, the epithelial cells derived from kidney organoids are dissociated and reconstructed tubular structure in the organ-on-a-chip, and permeability assay are realized using this platform.[55] Application of the epithelial cells in the gut-organoids to our new 3D gut model will allow for a drug screening system for assessing the effects on gut epithelial functions from the lumen side.

Conflicts of interest

There are no conflicts to declare.

Acknowledgments

We thank Maki Yamaguchi, Sumitomo Chemical Co., Ltd., for her technical assistance in the TEM analysis, Eri Otsuka for her technical assistance in the device fabrication, and Masayoshi Kobayashi and Yasushi Kuromi, SCREEN Holdings Co., Ltd., for their technical assistance on OCT imaging. This research was partly supported by MEXT/JSPS Kakenhi to T.N. (JP19K16177).

Biomaterials Science Accepted Manuscript

View Article Online
DOI: 10.1039/D0BM00763C

Published on 31 August 2020. Downloaded by The University of Tokyo on 9/16/2020 10:48:37 AM.

References

1 A. M. Chin, D. R. Hill, M. Aurora and J. R. Spence, *Semin. Cell Dev. Biol.*, 2017, **66**, 81–93.

2 E. Salvo Romero, C. Alonso Cotoner, C. Pardo Camacho, M. Casado Bedmar and M. Vicario, *Rev. Española Enfermedades Dig.*, 2015, **108**, 686–695.

3 C. L. Boulangé, A. L. Neves, J. Chilloux, J. K. Nicholson and M. E. Dumas, *Genome Med.*, 2016, **8**, 1–12.

4 C. R. Jones, O. J. D. Hatley, A. L. Ungell, C. Hilgendorf, S. Annie and A. Rostami-Hodjegan, *AAPS J.*, 2016, **18**, 589–604.

5 P. Artursson and J. Karlsson, *Biochem. Biophys. Res. Commun.*, 1991, **175**, 880–885.

6 S. HILARY, A. Francisco, A. M. Jose, K. Jaleel, S. Usama, S. AL H, H. Hosam, I. Wissam and P. Carine, *Food Chem.*, 2020, **311**, 125969.

7 L. Dreyer, C. Smith, S. M. Deane, L. M. T. Dicks and A. D. van Staden, *Sci. Rep.*, 2019, **9**, 1–11.

8 Y. Kamiya, H. Takaku, R. Yamada, C. Akase, Y. Abe, Y. Sekiguchi, N. Murayama, M. Shimizu, M. Kitajima, F. Shono, K. Funatsu and H. Yamazaki, *Toxicol. Reports*, 2020, **7**, 149–154.

9 S. Yamashita, K. Konishi, Y. Yamazaki, Y. Taki, T. Sakane, H. Sezaki and Y. Furuyama, *J. Pharm. Sci.*, 2002, **91**, 669–679.

10 R. L. DiMarco, D. R. Hunt, R. E. Dewi and S. C. Heilshorn, *Biomaterials*, 2017, **129**, 152–162.

11 A. A. M. Kämpfer, P. Urbán, S. Gioria, N. Kanase, V. Stone and A. Kinsner-Ovaskainen, *Toxicol. Vitr.*, 2017, **45**, 31–43.

12 J. Zhang, J. Penny and J. R. Lu, *Int. J. Food Sci. Nutr.*, 2019, 1–14.

13 H. Clevers, *Cell*, 2013, **154**, 274.

14 D. W. M. Tan and N. Barker, *Intestinal Stem Cells and Their Defining Niche*, Elsevier Inc., 1st edn., 2014, vol. 107.

Biomaterials Science Accepted Manuscript

View Article Online
DOI: 10.1039/D0BM00763C

Published on 31 August 2020. Downloaded by The University of Tokyo on 9/16/2020 10:48:37 AM.

15 S. W. Crawley, M. S. Mooseker and M. J. Tyska, *J. Cell Biol.*, 2014, **207**, 441–451.

16 K. Schneeberger, S. Roth, E. E. S. Nieuwenhuis and S. Middendorp, *DMM Dis. Model. Mech.*, 2018, **11**, dmm031088.

17 H. J. Kim, D. Huh, G. Hamilton and D. E. Ingber, *Lab Chip*, 2012, **12**, 2165–2174.

18 H. J. Kim and D. E. Ingber, *Integr. Biol. (United Kingdom)*, 2013, **5**, 1130–1140.

19 H. J. Kim, H. Li, J. J. Collins and D. E. Ingber, *Proc. Natl. Acad. Sci. U. S. A.*, 2016, **113**, E7–E15.

20 S. Jalili-Firoozinezhad, F. S. Gazzaniga, E. L. Calamari, D. M. Camacho, C. W. Fadel, A. Bein, B. Swenor, B. Nestor, M. J. Cronce, A. Tovaglieri, O. Levy, K. E. Gregory, D. T. Breault, J. M. S. Cabral, D. L. Kasper, R. Novak and D. E. Ingber, *Nat. Biomed. Eng.*, 2019, **3**, 520–531.

21 I. Okayasu, S. Hatakeyama, M. Yamada, T. Ohkusa, Y. Inagaki and R. Nakaya, *Gastroenterology*, 1990, **98**, 694–702.

22 W. Shin and H. J. Kim, *Proc. Natl. Acad. Sci. U. S. A.*, 2018, **115**, E10539–E10547.

23 X. Deng, G. Zhang, C. Shen, J. Yin and Q. Meng, *Appl. Microbiol. Biotechnol.*, 2013, **97**, 6943–6955.

24 S. Sibilio, V. De Gregorio, F. Urciuolo, P. A. Netti and G. Imparato, *Mater. Today Bio*, 2019, **4**, 100027.

25 T. T. Roh, Y. Chen, H. T. Paul, C. Guo and D. L. Kaplan, *Biomaterials*, 2019, **225**, 119517.

26 A. E. Shyer, T. Tallinen, N. L. Nerurkar, Z. Wei, E. S. Gil, D. L. Kaplan, C. J. Tabin and L. Mahadevan, *Science (80-.).*, 2013, **342**, 212–218.

27 J. Pauty, R. Usuba, H. Takahashi, J. Suehiro, K. Fujisawa, K. Yano, T. Nishizawa and Y. T. Matsunaga, *Nanotheranostics*, 2017, **1**, 103–113.

28 J. Pauty, R. Usuba, I. G. Cheng, L. Hespel, H. Takahashi, K. Kato, M. Kobayashi, H. Nakajima, E. Lee, F. Yger, F. Soncin and Y. T. Matsunaga, *EBioMedicine*, 2018, **27**, 225–236.

Biomaterials Science Accepted Manuscript

View Article Online
DOI: 10.1039/D0BM00763C

Published on 31 August 2020. Downloaded by The University of Tokyo on 9/16/2020 10:48:37 AM.

29 R. Usuba, J. Pauty, F. Soncin and Y. T. Matsunaga, *Biomaterials*, 2019, **197**, 305–316.

30 H. Takahashi, K. Kato, K. Ueyama, M. Kobayashi, G. Baik, Y. Yukawa, J. I. Suehiro and Y. T. Matsunaga, *Sci. Rep.*, 2017, **7**, 1–10.

31 H. Koyama, D. Shi and T. Fujimori, *Biophys. Physicobiology*, 2019, **16**, 80–88.

32 A. Trushko, I. Di Meglio, A. Merzouki, C. Blanch-Mercader, S. Abuhattum, J. Guck, K. Alessandri, P. Nassoy, K. Kruse, B. Chopard and A. Roux, *bioRxiv*, 2019, 513119.

33 M. Tozluo, M. Duda, N. J. Kirkland, R. Barrientos, J. Mun and J. J. Burden, *Dev. Cell*, 2019, **51**, 299–312.

34 K. D. Sumigray, M. Terwilliger and T. Lechler, *Dev. Cell*, 2018, **45**, 183-197.e5.

35 M. Liu, Z. Zhang, L. Sampson, X. Zhou, K. Nalapareddy, Y. Feng, S. Akunuru, J. Melendez, A. K. Davis, F. Bi, H. Geiger and M. Xin, *Stem Cell Reports*, 2017, **9**, 1961–1975.

36 L. Azzolin, T. Panciera, S. Soligo, E. Enzo, S. Bicciato, S. Dupont, S. Bresolin, C. Frasson, G. Basso, V. Guzzardo, A. Fassina and M. Cordenonsi, *Cell*, 2014, **158**, 157–170.

37 F. Deng, L. Peng, Z. Li, G. Tan, E. Liang, S. Chen, X. Zhao and F. Zhi, *Cell Death Dis.*, 2018, **9**, 153.

38 S. Yui, L. Azzolin, M. Maimets, P. J. Schweiger, S. Piccolo, K. B. Jensen, S. Yui, L. Azzolin, M. Maimets, M. T. Pedersen, R. P. Fordham and S. L. Hansen, *Cell Stem Cell*, 2018, **22**, 35–49.

39 D. Serra, U. Mayr, A. Boni, I. Lukonin, M. Rempfler, L. C. Meylan, M. B. Stadler, P. Strnad, P. Papasaikas, D. Vischi, A. Waldt, G. Roma and P. Liberali, *Nature*, 2019, **569**, 66–72.

40 M. Aragona, T. Panciera, A. Manfrin, S. Giulitti, F. Michielin and N. Elvassore, *Cell*, 2013, **154**, 1047–1059.

41 C. Zihni, E. Vlassaks, S. Terry, J. Carlton, T. King, C. Leung, M. Olson, F. Pichaud, M. S. Balda and K. Matter, *Nat. Cell Biol.*, 2017, **19**, 1049–1060.

Biomaterials Science Accepted Manuscript

View Article Online
DOI: 10.1039/D0BM00763C

42 T. Hirashima and T. Adachi, *Development*, 2019, **146**, dev181206.

43 H. Gon, K. Fumoto, Y. Ku, S. Matsumoto and A. Kikuchi, *Mol. Cell. Biochem.*, 2013, **24**, 3764–3774.

44 J. Cre, R. Courson, T. Mangeat, J. Foncy, S. Souleille, C. Thibault, A. Besson and L. Malaquin, *Biomaterials*, 2019, **221**, 119404.

45 D. Khalipina, Y. Kaga, N. Dacher, N. R. Chevalier and N. R. Chevalier, *J. R. Soc. Interface*, 2019, **16**, 20190484.

46 R. R. Roberts, M. Ellis, R. M. Gwynne, A. J. Bergner, M. D. Lewis, E. A. Beckett, J. C. Bornstein and H. M. Young, *J. Physiol.*, 2010, **588**, 1153–1169.

47 V. De Gregorio, F. Urciuolo, B. Corrado, P. A. Netti, S. Sbrescia and G. Imparato, *Biotechnol. Bioeng.*, 2020, **117**, 556–566.

48 T. Sato, J. H. Van Es, H. J. Snippert, D. E. Stange, R. G. Vries, M. Van Den Born, N. Barker, N. F. Shroyer, M. Van De Wetering and H. Clevers, *Nature*, 2011, **469**, 415–418.

49 C. L. Watson, M. M. Mahe, J. Múnera, J. C. Howell, N. Sundaram, H. M. Poling, J. I. Schweitzer, J. E. Vallance, C. N. Mayhew, Y. Sun, G. Grabowski, S. R. Finkbeiner, J. R. Spence, N. F. Shroyer, J. M. Wells and M. A. Helmrath, *Nat. Med.*, 2014, **20**, 1310–1314.

50 H. Uchida, M. Machida, T. Miura, T. Kawasaki, T. Okazaki, K. Sasaki, S. Sakamoto, N. Ohuchi, M. Kasahara, A. Umezawa and H. Akutsu, *JCI Insight*, 2017, **2**, e86492.

51 N. Gjorevski, N. Sachs, A. Manfrin, S. Giger, M. E. Bragina, P. Ordóñez-Morán, H. Clevers and M. P. Lutolf, *Nature*, 2016, **539**, 560–564.

52 G. Altay, E. Larrañaga, S. Tosi, F. M. Barriga and E. Batlle, *Sci. Rep.*, 2019, **9**, 10140.

53 T. Takebe, B. Zhang and M. Radisic, *Cell Stem Cell*, 2017, **21**, 297–300.

54 S. E. Park, A. Georgescu and D. Huh, *Science*, 2019, **364**, 960–965.

Published on 31 August 2020. Downloaded by The University of Tokyo on 9/16/2020 10:48:37 AM.

Biomaterials Science Accepted Manuscript

View Article Online
DOI: 10.1039/D0BM00763C

55 F. Schutgens, M. B. Rookmaaker, T. Margaritis, A. Rios, C. Ammerlaan, J. Jansen, L. Gijzen, M. Vormann, A. Vonk, M. Viveen, F. Y. Yengej, S. Derakhshan, K. M. de Winter-de Groot, B. Artegiani, R. van Boxtel, E. Cuppen, A. P. A. Hendrickx, M. M. van den Heuvel-Eibrink, E. Heitzer, H. Lanz, J. Beekman, J. L. Murk, R. Masereeuw, F. Holstege, J. Drost, M. C. Verhaar and H. Clevers, *Nat. Biotechnol.*, 2019, **37**, 303–313.

Published on 31 August 2020. Downloaded by The University of Tokyo on 9/16/2020 10:48:37 AM.

Biomaterials Science Accepted Manuscript

View Article Online
DOI: 10.1039/D0BM00763C

Published on 31 August 2020. Downloaded by The University of Tokyo on 9/16/2020 10:48:37 AM.

Figure captions

Figure 1. Proposed *in vitro* 3D gut model using a ductal scaffold-based culture system. (A) Construction protocol for the 3D gut model. (B) Experimental design of this study. In comparison with 2D and 3D gut models, we characterized the morphological changes at the tissue level (i.e. crypt- and villus-like domains) and cellular level (i.e. microvilli, cellular height, and tight junction formation). Phenotypic analyses, such as permeability and absorption assays, were established using the 3D gut model and these functions were then compared in the 2D and 3D models.

Figure 2. Morphological changes of the epithelial tissue in the 3D gut model. (A) Time-course bright-field images of the 3D gut model. Arrows: area showing epithelial buckling. Scale bar: 500 μm. (B) Magnified image of the black square of (A). Scale bar: 200 μm. (C) Time-course 3D observation of the 3D or 2D gut model using optical coherence tomography (OCT) imaging system. Arrows: area showing epithelial buckling. (D) The ductal diameter and (E) epithelial thickness of the 3D gut model measured using the obtained OCT images. *: $p \leq 0.05$ compared with the 2D gut model. Different alphabet indicates $p \leq 0.05$ in time series groups of the 3D gut model. Dash line: original lumen diameter (300 μm) in the 3D model.

Figure 3. Localization of cell proliferating region in the 3D gut model observed by confocal microscope. (A) 3D images and maximum intensity projection images (MIP) images at X-Y plane of EdU assay in the 2D and 3D gut models cultured for 16 days. Red: EdU-positive nuclei. Blue: nuclei. Scale bar: 50 μm. (B) The ratio of cell proliferation calculated as (EdU-positive nuclei)/(all nuclei). *: $p \leq 0.05$. (C) The χ^2 values of the proliferating cells calculated in 9 sub-areas. A larger value indicates the distribution of the proliferating cells in a localized manner. (D) Maximum intensity projection (MIP) images at X-Y plane

Biomaterials Science Accepted Manuscript

View Article Online
DOI: 10.1039/D0BM00763C

Published on 31 August 2020. Downloaded by The University of Tokyo on 9/16/2020 10:48:37 AM.

and cross-sectional images at X-Z plane of phalloidin staining for detection of fibril actin (F-actin; green) in the 2D and 3D gut models cultured for 16 days. Nuclei were visualized with Hoechst 33343 (blue). In the 3D model, the apical surface of the cells was indicated as the white dot line. Scale bar: 50 μm. (E) The quantitative analysis of F-actin area in the 2D and 3D gut models cultured for 16 days. *: $p \leq 0.05$. (F) The mRNA expression of stemness and differential marker genes in the 2D and 3D gut model by qRT-PCR. *: $p \leq 0.05$. (G) Schematic image of the distribution of the proliferating cells and F-actin (green) in the 2D and 3D models.

Figure 4 Morphologically differentiated epithelial cells in the 3D gut model. (A) The transmission electron microscopy (TEM) images of CACO-2 cells cultured in the 2D and 3D models for 4 or 16 days. (B) Yellow squares and high-magnification images were highlighted as tight junctions. The top of the images showed the lumen side in the 2D and 3D model, whereas the bottom of images showed the filter membrane side in the 2D model and collagen gel side in the 3D model. Scale bar: 2 μm. Cellular height (C), aspect ratio (height/width) (D), and density of microvilli of CACO-2 cells (E) were measured in the TEM images. (F) The distribution of angles of microvilli divided into each 10° was listed as the maximum value, 90°. (G) The mean angles of microvilli were calculated. *: $p \leq 0.05$. (H) Schematic image of the morphology of the gut epithelial cells in the 2D and 3D models. Gray lines on the cell surface: microvilli. Red lines: tight junctions.

Figure 5 Phenotypic analysis of the intestinal physiological functions using the 3D gut model: a permeability assay mimicking barrier disruption that induces inflammation and absorption assay reflecting ingestive effects. (A) Permeability assay after dextran sodium sulfate (DSS) treatment. Bright-field images of the 3D gut models treated with 2% DSS from 12 to 16 days (upper). Fluorescent images at 20 min after

Biomaterials Science Accepted Manuscript

View Article Online
DOI: 10.1039/D0BM00763C

FITC-4 kDa dextran treatment in the 3D gut models treated with 2% DSS from 12 to 16 days (bottom). White dash line: the edge between the epithelial surface and lumen. Scale bar: 200 μm. (B) Time-course fluorescent intensity in the 2D and 3D gut models cultured for 16 days. *: $p \leq 0.05$ compared with the control. (C) Immunofluorescent images for ZO1 (green) in the 2D and 3D gut models cultured with or without 2% DSS from 12 to 16 days. Blue: nuclei. Scale bar: 20 μm (D) Absorption rate of αLA under the filter and in collagen gel (mol/mm^2 of cell surface) with or without 10 mM NaN_3 treatment in 2D and 3D gut models cultured for 16 days, respectively. *: $p \leq 0.05$. (E) Schematic image of absorption function in the 2D and 3D models. The increase of surface at cellular and tissue levels may be due to the increase of the amount of absorption/unit epithelial area.

Published on 31 August 2020. Downloaded by The University of Tokyo on 9/16/2020 10:48:37 AM.

Biomaterials Science Accepted Manuscript

View Article Online
DOI: 10.1039/D0BM00763C

Published on 31 August 2020. Downloaded by The University of Tokyo on 9/16/2020 10:48:37 AM.

Figures

Figure 1

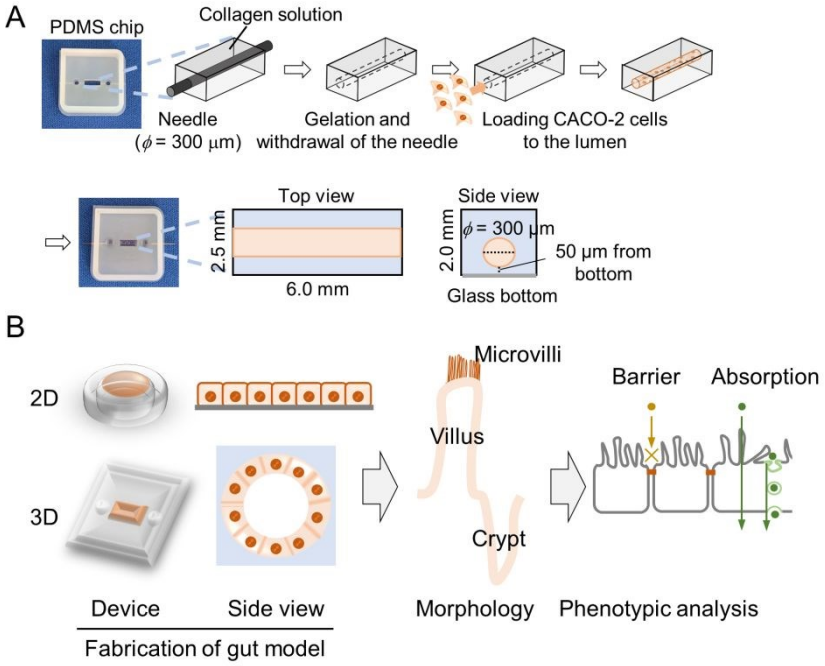

Biomaterials Science Accepted Manuscript

View Article Online
DOI: 10.1039/D0BM00763C

Published on 31 August 2020. Downloaded by The University of Tokyo on 9/16/2020 10:48:37 AM.

Figure 2

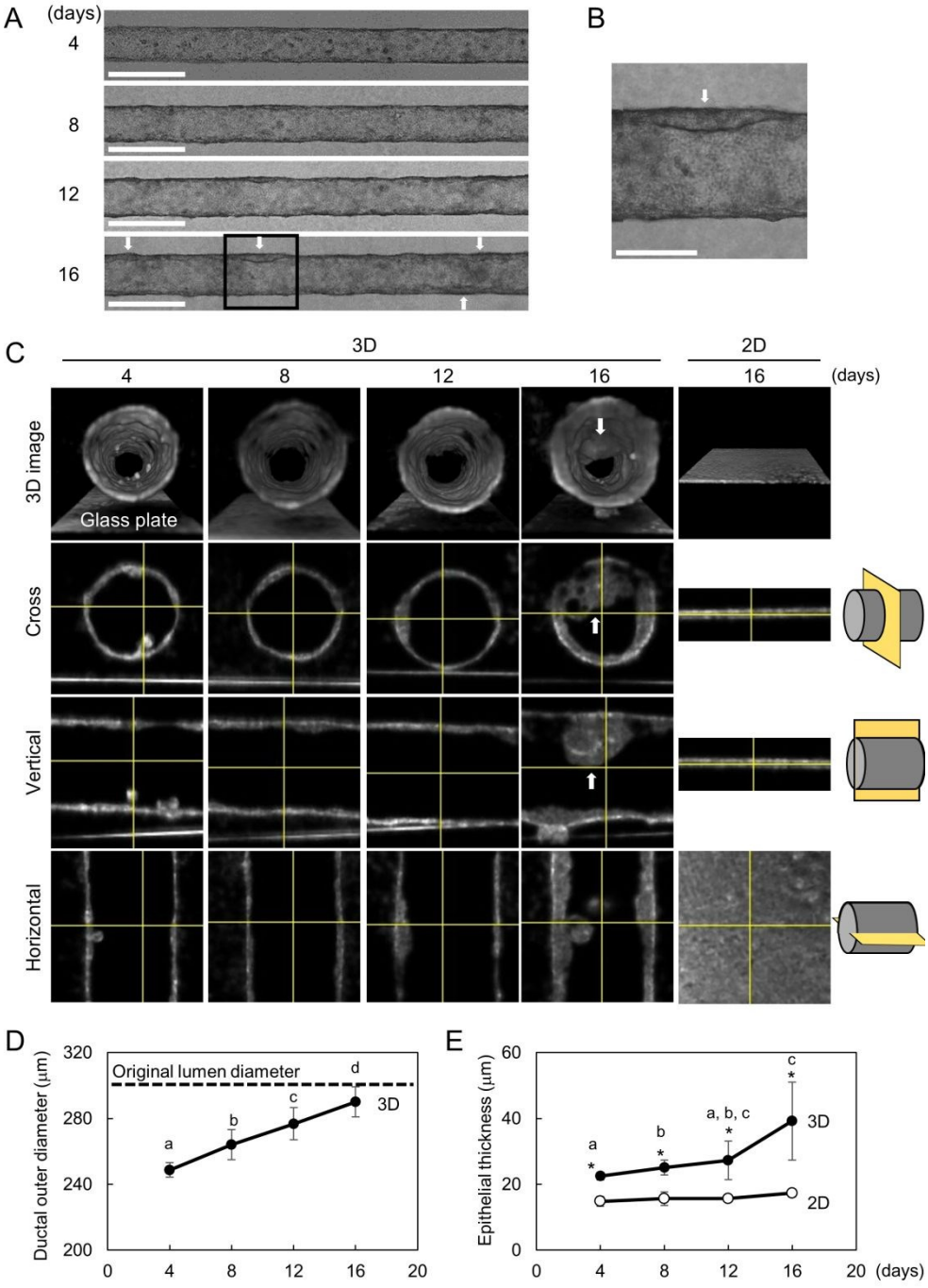

Biomaterials Science Accepted Manuscript

View Article Online
DOI: 10.1039/D0BM00763C

Published on 31 August 2020. Downloaded by The University of Tokyo on 9/16/2020 10:48:37 AM.

Figure 3

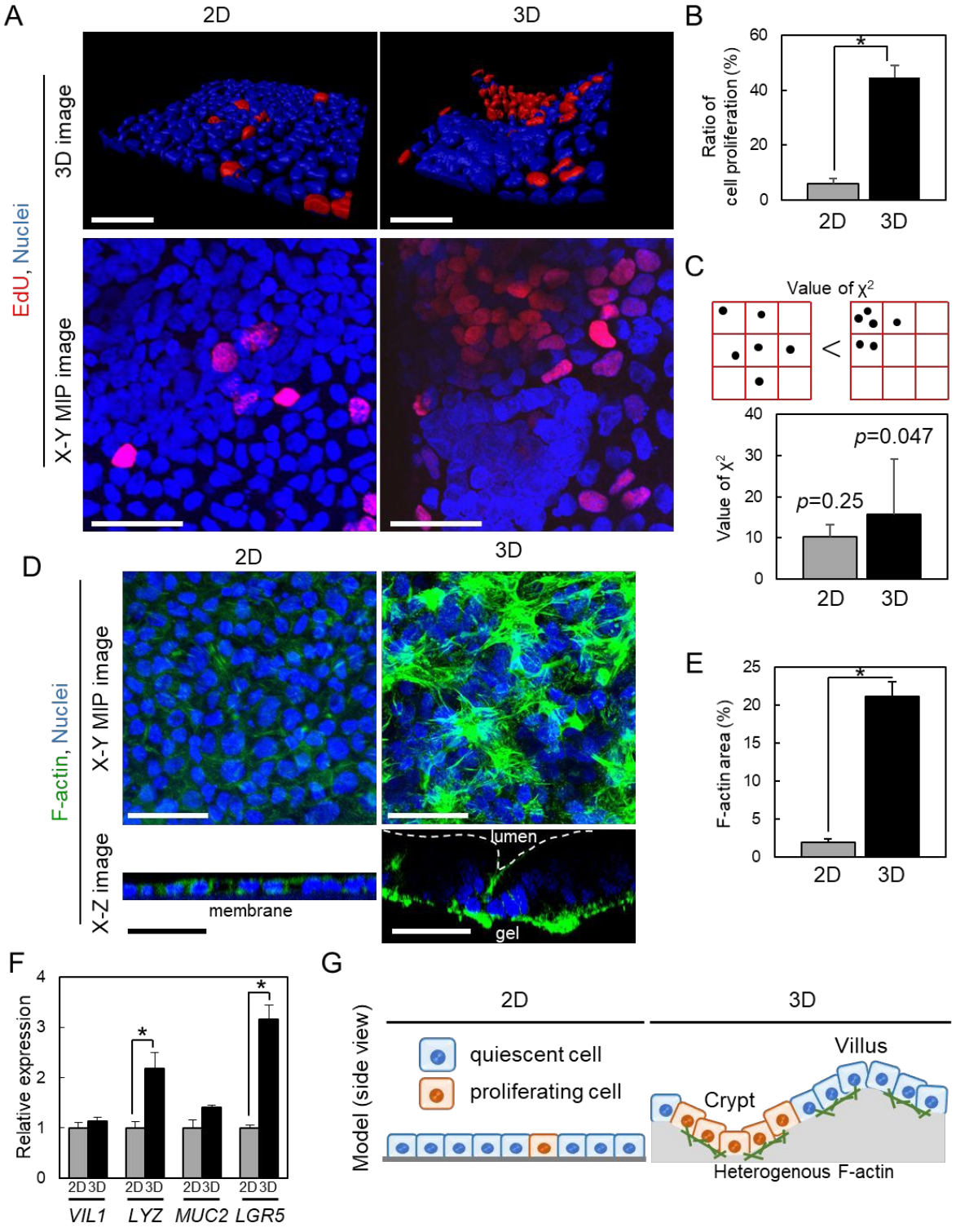

Biomaterials Science Accepted Manuscript

View Article Online
DOI: 10.1039/D0BM00763C

Published on 31 August 2020. Downloaded by The University of Tokyo on 9/16/2020 10:48:37 AM.

Figure 4

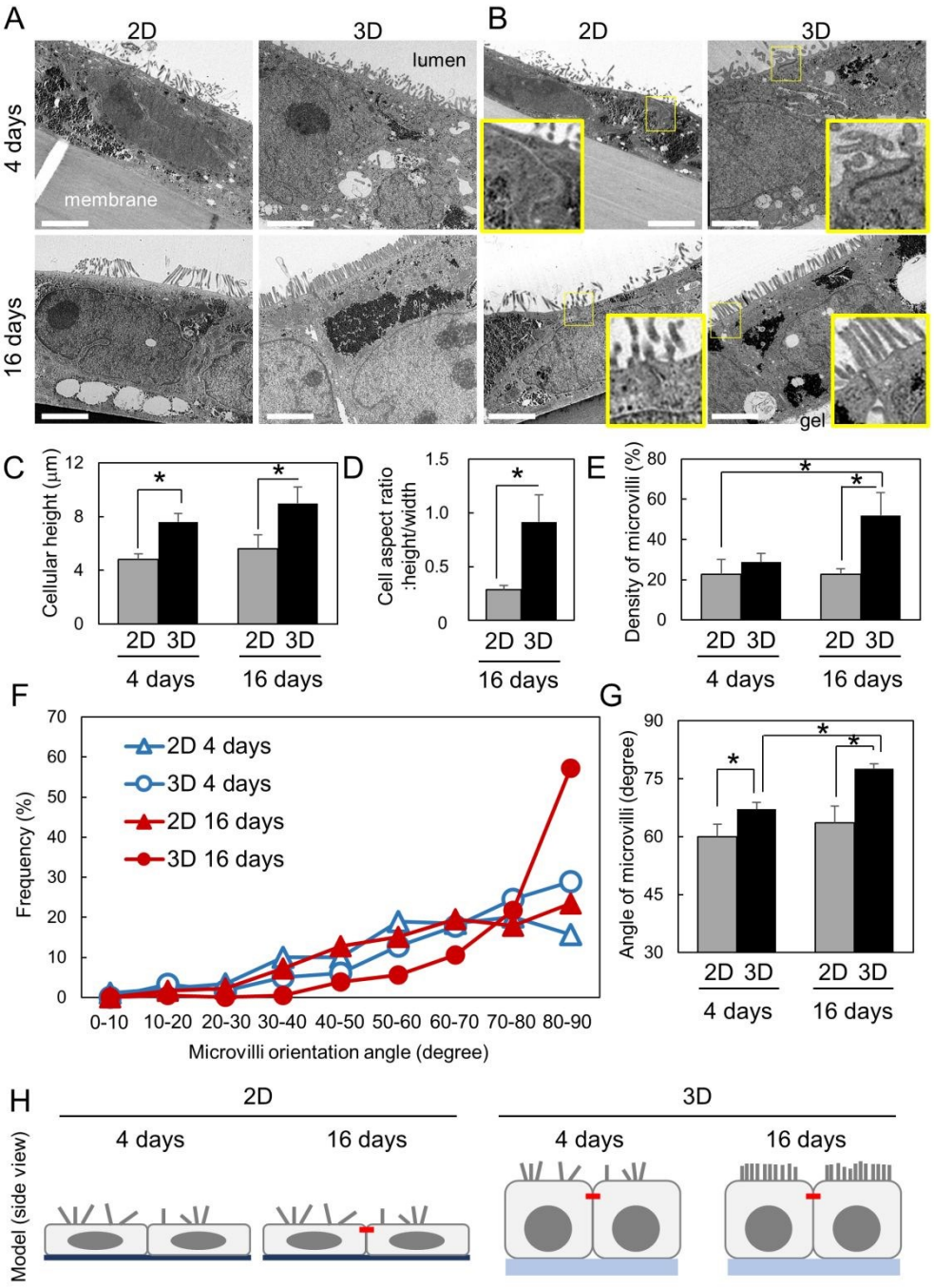

Biomaterials Science Accepted Manuscript

View Article Online
DOI: 10.1039/D0BM00763C

Published on 31 August 2020. Downloaded by The University of Tokyo on 9/16/2020 10:48:37 AM.

Figure 5

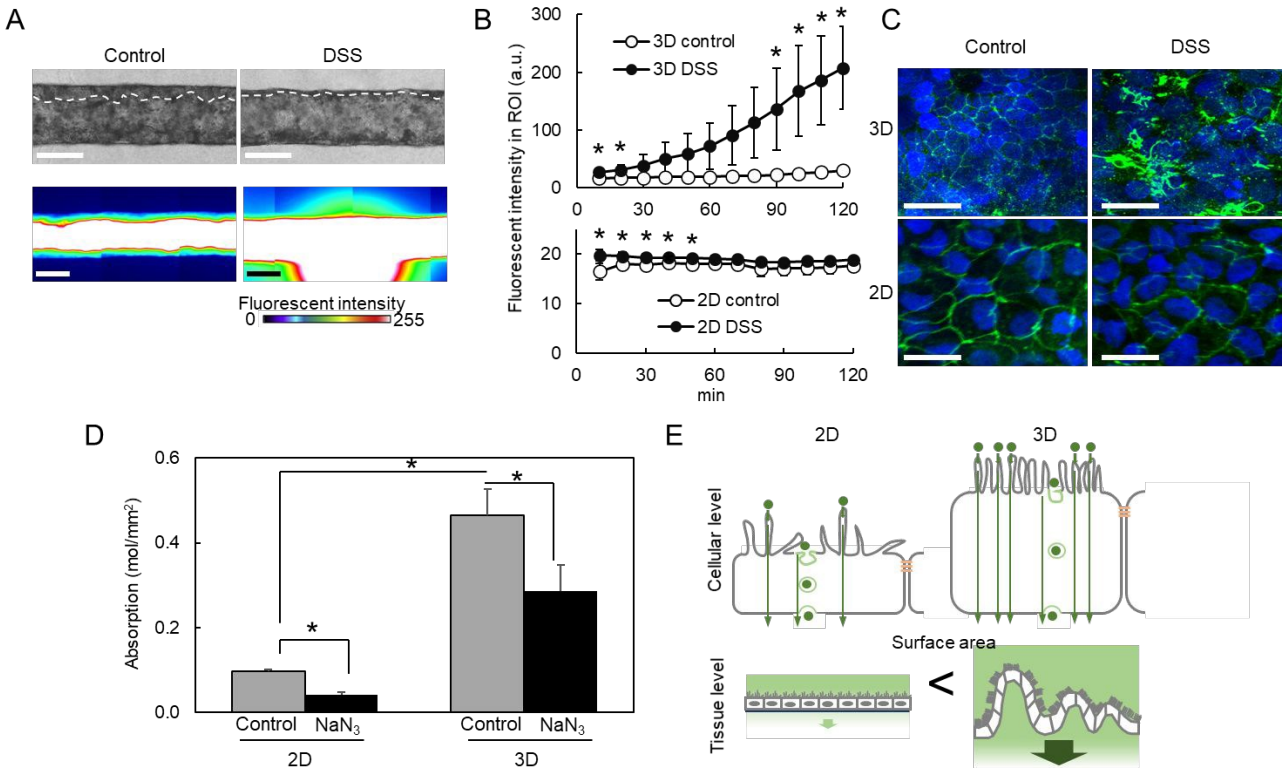

Biomaterials Science Accepted Manuscript

View Article Online
DOI: 10.1039/D0BM00763C

Graphical abstract

Tadaaki Nakajima[1], Katsunori Sasaki[2], Akihiro Yamamori[2], Kengo Sakurai[2], Kaori Miyata[2], Tomoyuki Watanabe[2], Yukiko T. Matsunaga[1*].

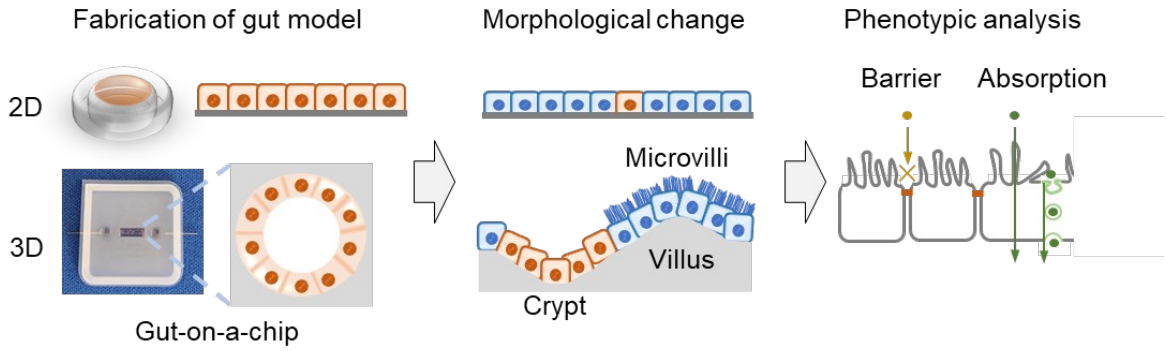

A new 3D gut-on-a-chip on the ductal scaffold induced differentiated epithelial layer and allowed permeability and absorption assay.

Published on 31 August 2020. Downloaded by The University of Tokyo on 9/16/2020 10:48:37 AM.

Biomaterials Science Accepted Manuscript